JGR Planets

RESEARCH ARTICLE
10.1029/2023JE008179

Key Points:
- Ilmenite reduction experiments were run at a wide range of experimental conditions
- Subsolidus reduction of ilmenite under lunar conditions creates magnetizable products
- Some swirl magnetic source bodies may be caused by cooling high-Ti basaltic dikes

Supporting Information:

Supporting Information may be found in the online version of this article.

Correspondence to:

Y. Liang,
yuanyuanliang@wustl.edu

Citation:

Liang, Y., Tikoo, S. M., & Krawczynski, M. J. (2024). Possibility of lunar crustal magmatism producing strong crustal magnetism. *Journal of Geophysical Research: Planets*, *129*, e2023JE008179. https://doi.org/10.1029/2023JE008179

Received 26 OCT 2023
Accepted 6 MAY 2024

Author Contributions:

Conceptualization: Y. Liang, S. M. Tikoo, M. J. Krawczynski
Data curation: Y. Liang
Formal analysis: Y. Liang, S. M. Tikoo, M. J. Krawczynski
Funding acquisition: S. M. Tikoo, M. J. Krawczynski
Investigation: Y. Liang, S. M. Tikoo, M. J. Krawczynski
Methodology: Y. Liang, S. M. Tikoo, M. J. Krawczynski
Project administration: S. M. Tikoo, M. J. Krawczynski
Resources: S. M. Tikoo, M. J. Krawczynski
Supervision: S. M. Tikoo, M. J. Krawczynski
Validation: S. M. Tikoo, M. J. Krawczynski
Visualization: S. M. Tikoo, M. J. Krawczynski
Writing – original draft: Y. Liang, S. M. Tikoo, M. J. Krawczynski
Writing – review & editing: Y. Liang, S. M. Tikoo, M. J. Krawczynski

Possibility of Lunar Crustal Magmatism Producing Strong Crustal Magnetism

Y. Liang[1], S. M. Tikoo[2], and M. J. Krawczynski[1]

[1]Department of Earth and Planetary Sciences, Washington University in St. Louis, St. Louis, MO, USA, [2]Department of Geophysics, Stanford University, Stanford, CA, USA

Abstract The Moon generated a long-lived core dynamo magnetic field, with intensities at least episodically reaching ∼10–100 μT during the period prior to ∼3.56 Ga. While magnetic anomalies observed within impact basins are likely attributable to the presence of impactor-added metal, other anomalies such as those associated with lunar swirls are not as conclusively linked to exogenic materials. This has led to the hypothesis that some anomalies may be related to magmatic features such as dikes, sills, and laccoliths. However, basalts returned from the Apollo missions are magnetized too weakly to produce the required magnetization intensities (>0.5 A/m). Here, we test the hypothesis that subsolidus reduction of ilmenite within or adjacent to slowly cooled mafic intrusive bodies could locally enhance metallic FeNi contents within the lunar crust. We find that reduction within hypabyssal dikes with high-Ti or low-Ti mare basalt compositions can produce sufficient FeNi grains to carry the minimum >0.5 A/m magnetization intensity inferred for swirls, especially if ambient fields are >10 μT or if fine-grained Fe-Ni metals in the pseudo-single domain grain size range are formed. Therefore, there exists a possibility that certain magnetic anomalies exhibiting various shapes such as linear, swarms, and elliptical patterns may be magmatic in origin. Our study highlights that the domain state of the magnetic carriers is an under-appreciated factor in controlling a rock's magnetization intensity. The results of this study will help guide interpretations of lunar crustal field data acquired by future rovers that will traverse lunar magnetic anomalies.

Plain Language Summary While the Moon does not have a magnetic field today, some parts of its crust such as impact basins and bright and sinuous features called "lunar swirls" are still magnetized. Strongly magnetized regions observed within impact basins could be related to iron-rich material derived from impactors. However, other magnetized regions, such as those associated with lunar swirls, are not as conclusively linked to externally added materials. It has been proposed that the strongly magnetic regions associated with lunar swirls are related to lunar igneous intrusive rocks. Here, we experimentally test the hypothesis that the thermal alteration of $FeTiO_3$ grains to TiO_2 grains and metallic iron within or next to slowly cooled igneous intrusive features while the Moon had a magnetic field, could explain the strong magnetic regions associated with lunar swirl. We show that the lunar swirl minimum magnetization intensity can be reached from the thermal alteration of ilmenite, especially if ambient fields are strong enough or if fine-grained Fe-Ni metals are formed. This study will help interpret data acquired by future rovers traversing magnetic anomalies on the lunar surface.

1. Introduction

Paleomagnetic studies have suggested that the Moon may have generated a core dynamo magnetic field at least intermittently between ∼4.25 and ∼1.5 Ga, with intensities reaching ∼40–110 μT prior to ∼3.56 Ga (Tikoo & Evans, 2022; Weiss & Tikoo, 2014; Wieczorek et al., 2023). The absence of magnetization within young lunar breccias suggests that the dynamo likely ceased between 1.92 and 0.80 Ga ago (Mighani et al., 2020). Whether the dynamo operated continuously and exactly when the lunar dynamo ceased remain uncertain (Evans et al., 2018; Tarduno et al., 2021). The dynamo history of the Moon is also evident from its remanent crustal magnetism (Hood, 2011; Hood et al., 2021; Purucker et al., 2012; Wieczorek et al., 2023). Intense magnetic anomalies within impact basins are likely caused by impactor-added metal within melt sheets (Oliveira et al., 2017), but anomalies associated with lunar swirls such as the archetypal Reiner Gamma (Denevi et al., 2016; Hemingway & Garrick-Bethell, 2012; Oliveira et al., 2024) and Airy albedo features (Blewett et al., 2011) are more difficult to unequivocally attribute to exogenic metal.

The bulk of remanent magnetization on the Moon is likely recorded within grains of metallic iron and iron-nickel alloys within crustal and upper mantle rocks (Weiss & Tikoo, 2014; Wieczorek, 2018). Anomalies on the

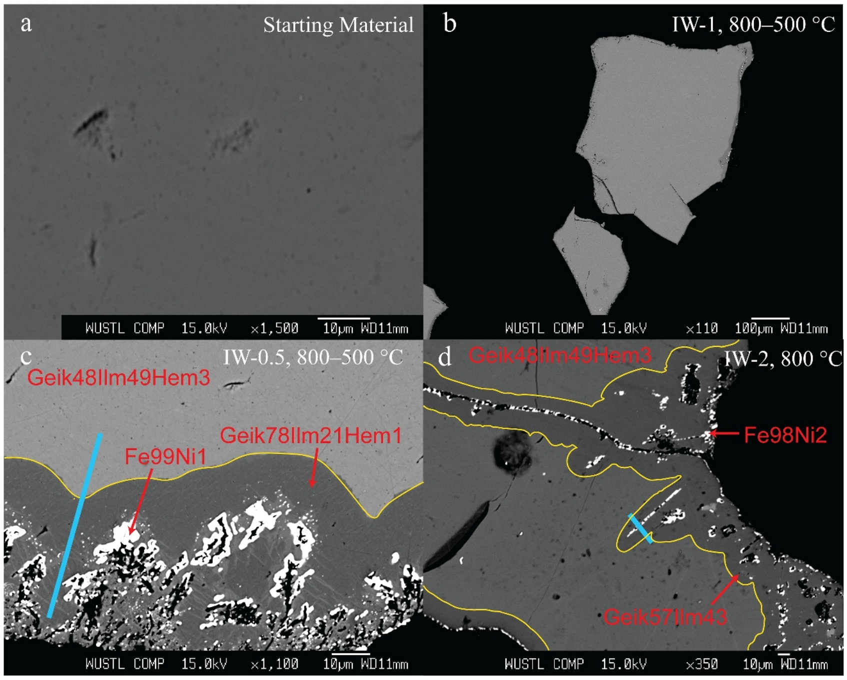

D . 3D 5 / 3 5
- . ' ' & 3 5D . ' &
/ 0 A R 3O % / A' ' ' P - P 4 5 & -
% 3 5D . / 0 B
3O % / A' ' ' P - P 4 5 7 8
- - - & & & 1
H & 1 . 1
- % 1 & . 3-
5 3 5D . / 0 A3O % / A' P 5
& 3 5

& & & % - 0 % &
& - & % 3 , & N5 % %
3 @B 5 & - / 37 5

3((

/ & % % / - &
2 1 & C - .
C %& - . % 2 & & .
- D & O
& / / &
- & C% & - E
P / & 0 % / /
O / & % / / 7 - E
& ' ' O

- / & K3 5 /
O 3 5 O 3 5 & O -
1 3 - 5 / / % % 3 - 5
/ / % - 3
@B & ' ' A5 . / & /
& - % 3 & ' ' A5 /
/ - & 1

10.1029/2023JE008179

Table 1
Run Conditions and Hysteresis Analyses of Starting Materials and Experimental Run Products

Exp	Temp (°C)	fO_2	Duration (days)	Ilmenite diameter (mm)	M_s (Am^2/kg)	M_{rs} (Am^2/kg)	M_{rs}/M_s	B_c (mT)	B_{cr} (mT)	B_{cr}/B_c	Geik	Ilm	Hem	Hysteresis mass (mg)
S.M.				~1–3	n/a	0.00	n/a	0.00	n/a	n/a	48.65	48.77	2.58	34
H155	800	IW-1	16	~1–3	3.43×10^{-2}	1.65×10^{-3}	4.81×10^{-2}	16.90	174.00	10.30	52.41	45.79	1.80	14
H154	800	IW-1	4	~1–3	3.20×10^{-2}	2.50×10^{-3}	7.80×10^{-2}	17.70	75.00	4.24				21
H158	800	IW-2	4	~1–3	1.94	5.24×10^{-2}	2.70×10^{-2}	2.30	22.00	9.57	57.17	43.10	0.00	28
J137	800	IW-1	8	~1–3	7.31×10^{-3}	8.23×10^{-4}	1.13×10^{-1}	18.40	62.00	3.37	50.95	49.44	0.00	32
J138	800	IW-1	2	~1–3	5.50×10^{-3}	1.17×10^{-3}	2.13×10^{-1}	27.10	300.00	11.07	50.33	46.32	3.35	17
H171	800–500	IW-0.5	6.2	~1–3 (3), ~0.5 (10)	8.13	6.50×10^{-1}	8.01×10^{-2}	4.10	10.00	2.44	78.43	21.00	0.57	9
H174	1000–500	IW-1	8.9	~1–3 (3), ~0.5 (15)	4.13×10^{-1}	1.20×10^{-2}	2.90×10^{-2}	4.80	47.00	9.79	51.15	48.43	0.41	10
H181_S	800–500	IW-1	6.2	0.86–0.47	4.78×10^{-1}	8.55×10^{-2}	1.79×10^{-1}	13.70	46.30	3.38	64.35	33.08	2.57	31
H181_M	800–500	IW-1	6.2	1.37–1.11	2.77×10^{-1}	4.91×10^{-2}	1.77×10^{-1}	16.30	53.20	3.26				31
H181_L	800–500	IW-1	6.2	3.97–1.96	2.40×10^{-1}	4.50×10^{-2}	1.88×10^{-1}	8.70	33.60	3.86				31
H182_S	800–500	IW-1	6.2	1.09–0.52	1.41	1.33×10^{-1}	9.43×10^{-2}	6.00	14.80	2.47	62.11	34.22	3.66	19
H182_M	800–500	IW-1	6.2	1.61–1.23	8.41×10^{-1}	8.15×10^{-2}	9.69×10^{-2}	5.30	27.00	5.09	62.21	34.78	3.01	31
H182_L	800–500	IW-1	6.2	3.97–1.96	6.66×10^{-1}	6.08×10^{-2}	9.13×10^{-2}	4.80	16.60	3.46				31

Note. S.M. stands for starting material. Experimental runs H171 and H174 were held at 800 and 1000°C respectively for 48 hr then cooled to 500°C by 3°C/hr; experimental runs H181 and H182 were held at 800°C for 48 hr and then cooled by 3°C/hr to 500°C. Geikielite, ilmenite, and hematite compositions were approximated because they were calculated from EPMA spot analyses. See Supporting Information S1 on how Geik, Ilm, and Hem compositions were calculated.

For the first batch of experiments, all experiments were conducted at 800°C and $fO_2 = \text{IW-1}$ with different time duration (2, 4, 8, and 16 days). Ilmenite grain sizes for the first batch of experiments ranged between 1 and 3 mm. For the second batch of cooling experiments, we used multiple cooling paths. One experiment involved heating ilmenite at 800°C for 48 hr and then cooling it to 500°C at a rate of 3°C/hr ($fO_2 = \text{IW-0.5}$) (experimental run H171), while a second experiment in this batch involved heating at 1000°C for 48 hr and then cooling to 500°C at a rate of 3°C/hr ($fO_2 = \text{IW-1}$) (experimental run H174). The fO_2 sensor was removed before the temperature dropped below 800°C for the cooling experiments to protect the fO_2 sensor. The fO_2 sensor was only rated for below 1,200 mV and decreasing temperature would increase the absolute mV values to greater than 1,200 mV. In the third batch of experiments ilmenite grain sizes were systematically varied. In addition to 1–3 mm ilmenite chips, we also included 10–15 0.5 mm diameter ilmenite pieces in these two experiments. For the third batch of experiments with different grain sizes of ilmenite (experimental runs H181 and H182), all experiments were heated at 800°C for 48 hr and then cooled to 500°C at 3°C/hr ($fO_2 = \text{IW-1}$). The fO_2 sensor was removed before the temperature dropped below 800°C during these experiments as well. Since the degree of subsolidus reduction may depend on the exposed surface area to volume ratio of a given ilmenite grain, the starting materials for each set of experiments were divided into small, medium, and large to study the relationship between starting materials' grain sizes and magnetization properties. Experimental runs H181_S and H182_S involved ilmenite grain sizes ranging between 0.5 and 1.0 mm in diameter. Ilmenite grain sizes in runs H181_M and H181_M were between 1.2 and 1.6 mm in diameter. Finally, starting materials grain sizes in runs H181_L and H181_L ranged between ~2.0 and 4.0 mm in diameter. Table 1 summarized the run conditions including the initial temperature, duration, cooling rate, grain size, oxygen fugacity, and experimental temperatures for all experiments.

Rock magnetic experiments (magnetic hysteresis and backfield remanence) were performed on ilmenite starting material as well as reduced products using a LakeShore 8600 Vibrating Sample Magnetometer (VSM) instrument at the Institute for Rock Magnetism at the University of Minnesota. These experiments elucidate the grain size of magnetic minerals and the magnetization carrying capacity of a sample. During a magnetic hysteresis experiment, a sample was placed within a VSM in an initial zero field. The field (B) was increased to an intensity of +1 Tesla (T) in the positive direction before being reduced in intensity and then applied in the reverse direction to the same

Table 2
EPMA Analyses of Starting Materials and Experimental Run Products in Oxide Weight Percentage

	No. of analyses	SiO_2		TiO_2		Al_2O_3		Cr_2O_3		FeO		MnO		MgO		CaO		NiO		ZnO		Na_2O		K_2O		Total
S.M.	41	0.00	0.08	55.02	0.26	0.65	0.07	1.92	0.03	27.55	0.27	0.26	0.02	14.37	0.08	0.03	0.04	0.21	0.02	0.02	0.02					100.01
H155	4	0.07	0.18	56.12	1.05	0.58	0.21	2.03	0.60	25.83	1.08	0.26	0.02	14.44	0.23	0.04	0.01	0.75	1.17	0.04	0.02					100.16
H158	10	0.00	0.07	58.37	1.63	0.81	0.54	2.07	1.27	22.09	0.41	0.36	0.05	16.97	0.13	0.07	0.03	0.04	0.04	0.01	0.03					100.79
J137	3	0.00	0.01	57.42	1.89	0.48	0.42	1.83	1.29	25.42	0.17	0.27	0.02	14.98	0.23	0.03	0.01	0.12	0.01	0.01	0.02					100.50
J138	4	0.03	0.05	55.45	0.14	0.80	0.17	1.94	0.02	27.96	0.33	0.26	0.01	15.02	0.26	0.03	0.02	0.22	0.02	0.04	0.01					101.76
H171	6	0.00	0.02	61.37	0.70	0.50	0.17	1.95	0.38	11.96	0.76	0.48	0.03	23.84	0.67	0.02	0.01	0.03	0.01	0.03	0.03	0.02	0.01	0.00	0.00	100.17
H174	4	0.00	0.02	58.43	0.26	0.19	0.09	0.73	0.16	25.57	0.21	0.29	0.04	14.85	0.15	0.03	0.01	0.06	0.07	0.02	0.03	0.05	0.03	0.01	0.01	100.18
H181_S	3	0.00	0.08	58.82	0.20	0.51	0.11	1.63	0.58	20.10	0.49	0.31	0.03	19.01	1.00	0.02	0.01	0.00	0.01	−0.01	0.02	0.03	0.03	0.00	0.01	100.40
H182_S	9	0.00	0.03	57.71	0.75	0.87	0.51	2.19	0.70	20.57	0.90	0.31	0.03	18.18	0.56	0.01	0.01	0.02	0.01	0.03	0.03	0.01	0.02	0.00	0.00	99.87
H182_M	2	0.10	0.05	56.49	0.69	1.04	0.35	3.18	1.29	20.99	0.09	0.29	0.00	18.84	0.79	0.01	0.00	0.04	0.02	0.05	0.00	0.05	0.01	0.00	0.00	101.08

Note. All 41 EPMA points of the starting materials were reported in this table because of their homogeneity. For the reduction experiments, we reported the average compositions and their one standard deviation of the top 10% highest geikielite components of the total analyses of each experimental run. The analyses in this table were taken from the reaction zone on the grains. Columns on the right of each oxide were each oxide's one standard deviation from the number of analyses for each experimental run. The full EPM spot analyses of the starting materials and each experimental run can be found in Supporting Information S1. Experimental runs H154, H181_M, H181_L, and H182_L were not analyzed by the EPMA, but their hysteresis analyses were reported in Table 1.

Table 3
Metal Compositions (at.%) for Experiments That Formed >5 μm Metals

	No. of analyses	Fe[a]	Ni[a]
H158	12	97.99	2.01
H171	5	99.28	0.72
H182_M	7	98.38	1.62
H182_L	1	98.59	1.41

Note. The FeNi metals were all close to the bcc regime and not close to the fcc regime. See Supporting Information S1 on how Fe and Ni compositions were calculated. [a]These compositions were approximated because they were calculated from EPMA spot analyses that overlapped with ilmenite.

3.2. Reduction Isothermal Experiments (800°C) Time Series at Constant fO_2

The reduced experiments run for different experimental durations had M_{rs} values of 5.50×10^{-3} Am^2/kg (experimental run J138 for 2-day), 2.50×10^{-3} Am^2/kg (experimental run H154 for 4-day), 8.23×10^{-4} Am^2/kg (experimental run J137 for 8-day), and 1.65×10^{-3} Am^2/kg (experimental run H155 for 16-day). Following our initial IW-1 experiments, M_{rs} values increased substantially from the zero value of the starting material, indicating that kamacite was likely the created phase rather than taenite (the latter is paramagnetic at room temperature for <30% Ni). Within this batch of experiments, there was no obvious correlation between the M_{rs} values and the experimental durations (Figure 3). We posit that the observed variations in M_{rs} were most likely dominated by the nonuniform density of random internal fractures inherent in the starting material that can differ between subsamples.

3.3. Reduction Experiments With Slow Cooling

To study the actual cooling process of ilmenite in the Moon's crust, we conducted two cooling experiments from 800 to 500°C at fO_2 = IW-0.5 (experimental run H171) and 1000–500°C at fO_2 = IW-1 (experimental run H174). Despite the uncertainties on the fO_2 conditions (as this run was initially intended to take place at IW-1), H171 had M_{rs} values at least 1 order of magnitude higher than the other isothermal experiments, and H174 had M_{rs} values similar to the other isothermal experiments (Table 1). The origin of the high M_{rs} value of the fO_2 = IW-0.5 experiment was unclear, but it may be possible that the starting material for this experimental run included either smaller than average grain sizes or grains with a high degree of internal fracturing that could have yielded higher surface area to volume ratios for reduction to occur. Therefore, we conducted more experiments using the same temperature and oxygen fugacity conditions but with different ilmenite grain sizes to explore the latter possibility.

3.4. Reduction Experiments With Varying Grain Sizes of Starting Materials

To study the effect of surface area on the extent of ilmenite reduction and metal creation, we conducted two sets of cooling experiments from 800 to 500°C at fO_2 = IW-1 for three different ilmenite grain size ranges (experimental runs H181 and H182). In general, we found that, within each experimental set, the M_{rs} values decreased with increasing ilmenite grain size for both H181 and H182 (Figure 4).

We also compared the other two cooling experiments (experimental runs H171 and H174) and our most reducing isothermal experiment ran at fO_2 = IW-2 (experimental run H158) with experimental runs H181 and H182 (Table 1) to study the interplay between cooling rate and ilmenite grain size effecting on the magnetization properties of the reduction product. Experimental run H174 had the lowest M_{rs} values which might be attributable to its high starting temperature at 1000°C that could have led to the production of larger, more multidomain (MD) metal grains within the sample. Experimental run H171 had the highest M_{rs} values among all experiments. The M_{rs} values for the small (H181_S and H182_S) and medium (H181_M and H182_M) ilmenite grain size experiments were much higher than the experimental run H158's M_{rs} value, and the large ilmenite grain size (H181_L and H182_L) experiments' M_{rs} values were comparable to H158's M_{rs} value (Table 1). Although the oxygen fugacity of H158 was more reduced compared to experimental runs H171, H181, and H182, slow-cooled experiments still showed higher M_{rs} values with smaller grain sizes and comparable M_{rs} values with similar grain sizes. The reduction products, Fe and rutile, were larger and more visible in the BSE images of the slow-cooled experiments too (Figures 1c and 1d).

4. Discussion

4.1. Ilmenite Subsolidus Reduction Creates FeNi Metal

Reduction of ilmenite to rutile and FeNi metals was observed in some Apollo samples. For reduction products in Apollo crystalline rock samples, the metal phases consisted entirely of kamacite (El Goresy et al., 1972). There were two steps in the proposed subsolidus reduction reaction: (a) ulvöspinel reduced to ilmenite and metallic iron,

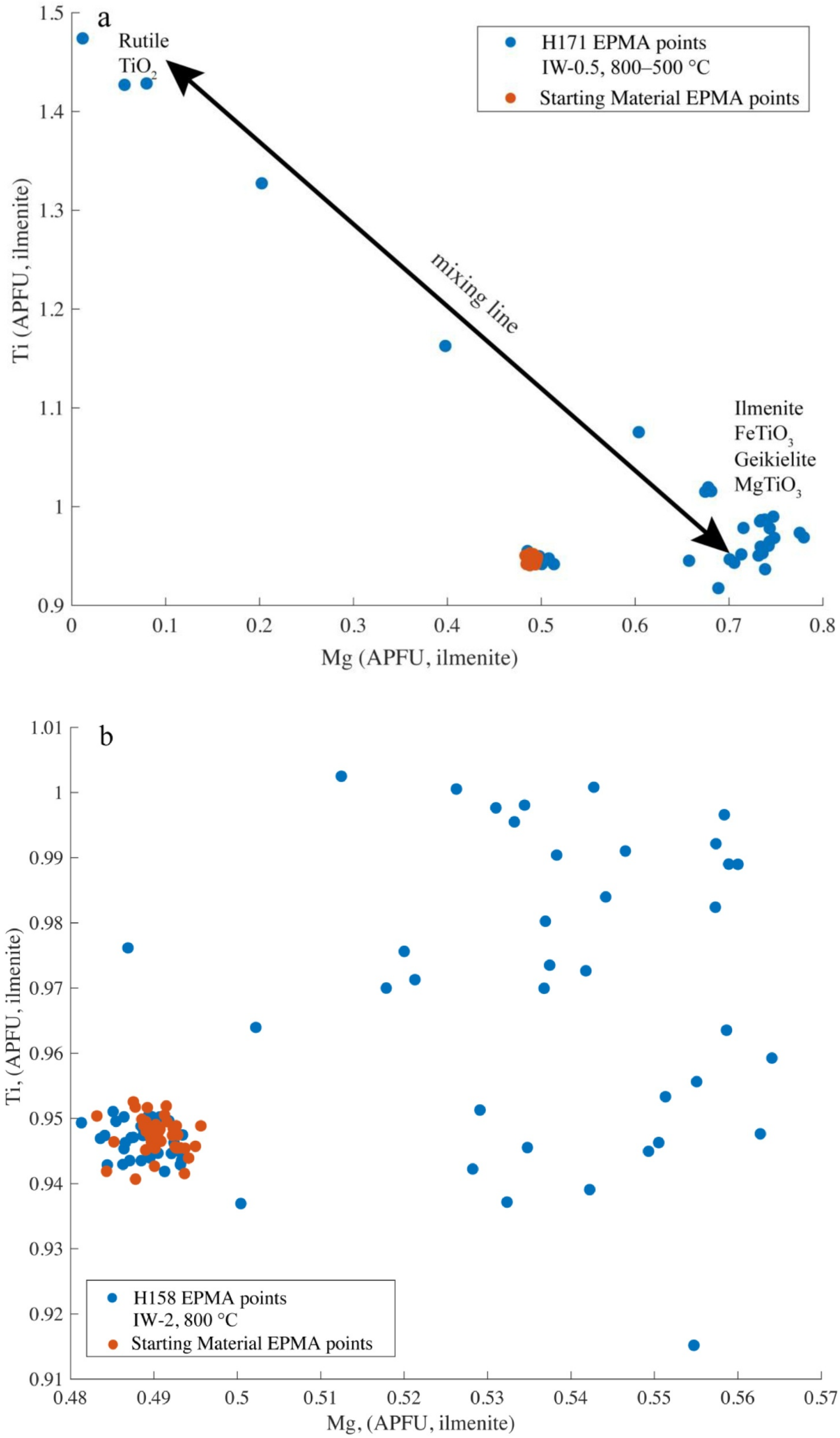
a
Rutile
TiO_2
H171 EPMA points
IW-0.5, 800–500 °C
Starting Material EPMA points
mixing line
Ilmenite
$FeTiO_3$
Geikielite
$MgTiO_3$
Ti (APFU, ilmenite)
Mg (APFU, ilmenite)
1.5
1.4
1.3
1.2
1.1
1
0.9
0
0.1
0.2
0.3
0.4
0.5
0.6
0.7
0.8
b
H158 EPMA points
IW-2, 800 °C
Starting Material EPMA points
Ti, (APFU, ilmenite)
Mg, (APFU, ilmenite)
1.01
1
0.99
0.98
0.97
0.96
0.95
0.94
0.93
0.92
0.91
0.48
0.49
0.5
0.51
0.52
0.53
0.54
0.55
0.56
0.57

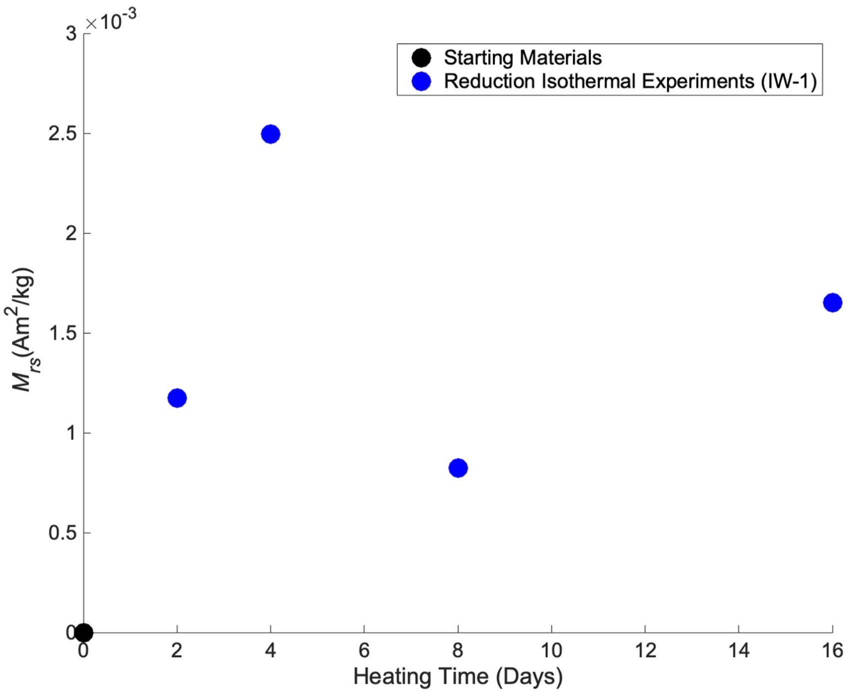
Starting Materials
Reduction Isothermal Experiments (IW-1)
M_{rs} (Am^2/kg)
×10^{-3}
3
2.5
2
1.5
1
0.5
0
0
2
4
6
8
10
12
14
16
Heating Time (Days)

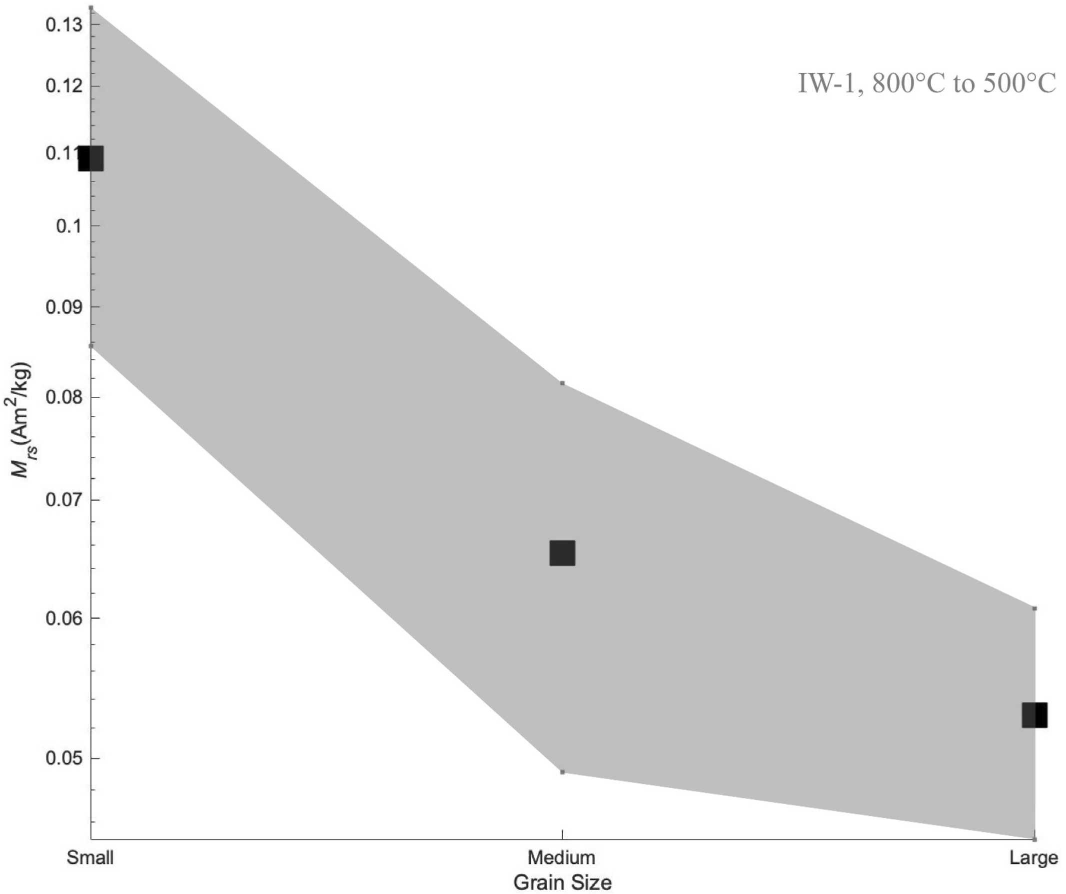
IW-1, 800°C to 500°C
0.13
0.12
0.11
0.1
0.09
0.08
0.07
0.06
0.05
M_{rs} (Am^2/kg)
Small
Medium
Large
Grain Size

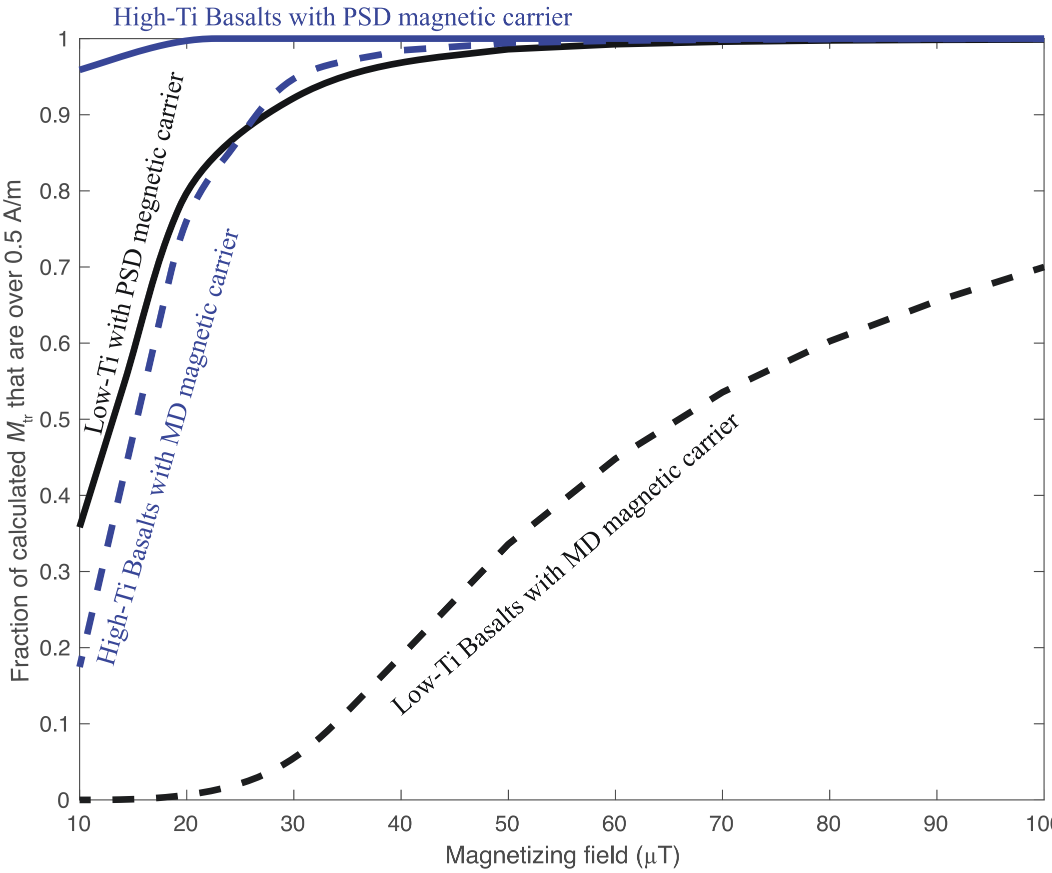

Figure 5. Different scenarios of percentages of calculated M_{tr} values that are over the minimum requirement for lunar swirls (0.5 A/m) with magnetizing field ranging from 10 to 100 μT with a dike width = 100 m. Blue line: high-Ti basalts with pseudo-single domain (PSD) magnetic carriers; blue dashed line: high-Ti basalts with multidomain magnetic carriers; black line: low-Ti basalts with PSD magnetic carriers; black dashed line: low-Ti basalts with multidomain magnetic carriers.

$$M_{tr} = \frac{c\ s\ B\ M_s^{Fe}}{a}, \tag{3}$$

where M_s^{Fe} was 1.715×10^6 A m^{-1} (Dunlop & Özdemir, 2015), and c was the volumetric concentration of Fe reduced from low-Ti and high-Ti mare basalts. The amounts of metallic Fe can be estimated by the reduction of ilmenite from low-Ti and high-Ti basalts using mass balance and densities. B ranged from 10 to 100 μT because ~100 μT was the upper limit of lunar paleointensities that had been inferred from paleomagnetic studies of Apollo samples. Constant a varied from ~2,810 μT for multidomain samples to ~3,770 μT for single-domain and pseudo-domain samples (Weiss & Tikoo, 2014; Wieczorek et al., 2023). The squareness s was the ratio of the saturation remanent magnetization (M_{rs}) and saturation magnetization (M_s) of the experimental samples and mare basalts. To understand the boundaries between domain states, we assumed $M_{rs}/M_s < 0.05$ was MD; between 0.05 and 0.5 was PSD, and >0.5 was SD (see Figure 7 of Strauss et al. (2021)). M_{rs}/M_s values from our experiments are listed in Table 1. We selected the experiments that were conducted under fO_2 = IW-1 and IW-2 and there were EPM analyses on the metallic irons (Table 3). The mean M_{rs}/M_s value from these experiments was 0.295 (PSD). We found that FeNi grains formed during our subsolidus reduction experiments were on average smaller (PSD; M_{rs}/M_s ~0.1) (Table 1) than those naturally occurring within mare basalts (multidomain; M_{rs}/M_s ~0.001–0.01). A typical M_{rs}/M_s value for mare basalts was ~0.0064 (Fuller & Cisowski, 1987). This was of interest because PSD grains can more efficiently record thermal remanent magnetization than multidomain grains for a given ambient field intensity (Figure 5). We noted that in a natural setting, protracted cooling on timescales far exceeding the durations of our laboratory experiments may result in the growth of MD grains rather than PSD grains. While it